Adaptor protein-3 complex is required for Vangl2 trafficking and planar cell polarity of the inner ear

Cristy Tower-Gilchrist[a,*], Stephanie A. Zlatic[a], Dehong Yu[a,b], Qing Chang[a,c], Hao Wu[b], Xi Lin[a,c], Victor Faundez[a], and Ping Chen[a,*]

[a]Department of Cell Biology and [c]Department of Otolaryngology, Emory University School of Medicine, Atlanta, GA 30322; [b]Department of Otolaryngology–Head and Neck Surgery, Xinhua Hospital and Ear Institute, Shanghai Jiaotong University School of Medicine, Shanghai 200125, China

ABSTRACT **Planar cell polarity (PCP) regulates coordinated cellular polarity among neighboring cells to establish a polarity axis parallel to the plane of the tissue. Disruption in PCP results in a range of developmental anomalies and diseases. A key feature of PCP is the polarized and asymmetric localization of several membrane PCP proteins, which is essential to establish the polarity axis to orient cells coordinately. However, the machinery that regulates the asymmetric partition of PCP proteins remains largely unknown. In the present study, we show Van gogh-like 2 (Vangl2) in early and recycling endosomes as made evident by colocalization with diverse endosomal Rab proteins. Vangl2 biochemically interacts with adaptor protein-3 complex (AP-3). Using short hairpin RNA knockdown, we found that Vangl2 subcellular localization was modified in AP-3–depleted cells. Moreover, Vangl2 membrane localization within the cochlea is greatly reduced in AP-3–deficient *mocha* mice, which exhibit profound hearing loss. In inner ears from AP-3–deficient *mocha* mice, we observed PCP-dependent phenotypes, such as misorientation and deformation of hair cell stereociliary bundles and disorganization of hair cells characteristic of defects in convergent extension that is driven by PCP. These findings demonstrate a novel role of AP-3–mediated sorting mechanisms in regulating PCP proteins.**

Monitoring Editor
Keith E. Mostov
University of California, San Francisco

Received: Aug 16, 2016
Revised: Jun 24, 2019
Accepted: Jun 28, 2019

INTRODUCTION

Planar cell polarity (PCP) refers to the coordinated polarization of neighboring cells along an axis parallel to the plane of the tissue. PCP is critical for tissue development and function. Defects in PCP lead to a range of developmental anomalies and diseases, including cancers and developmental defects in the neural tube, the inner ear, heart, and kidney (Veeman *et al.*, 2003; Guo *et al.*, 2004; Park *et al.*, 2006; Wang *et al.*, 2006a,b). Many of these diseases are direct results of loss of coordinated polarity of cells or defective convergent extension (CE), which is driven by polarized cellular rearrangements under the regulation of PCP signaling (Wallingford and Harland, 2002; Wang *et al.*, 2005; Axelrod, 2009).

The PCP pathway consists of a set of transmembrane proteins and their associated cytoplasmic proteins known as core PCP proteins, including Van gogh-like 1 and 2 (Vangl1 and Vangl2), Frizzled 3/6 (Fz3/Fz6), Dishevelled (Dvl), and Prickle (Pk) proteins (Axelrod, 2009; McNeill, 2010). These core PCP proteins are asymmetrically distributed within individual cells during PCP regulation. In the cochlea, the core PCP proteins are distributed in a polarized manner along the PCP axis in the terminally differentiated sensory epithelium known as the organ of Corti (Wang *et al.*, 2006b; Montcouquiol *et al.*, 2008). The core PCP proteins presumably form membrane-associated protein complexes at cellular boundaries to coordinate the polarity among neighboring cells (Guo *et al.*, 2004;

This article was published online ahead of print in MBoC in Press (http://www.molbiolcell.org/cgi/doi/10.1091/mbc.E16-08-0592) on July 3, 2019.

*Address correspondence to: Cristy Tower-Gilchrist (cristy.tower-gilchrist@emory.edu) or Ping Chen (ping.chen@emory.edu).

Abbreviations used: ABR, auditory brainstem response; AP-3, adaptor protein-3 complex; CE, convergent extension; co-IP, coimmunoprecipitation; DMSO, dimethyl sulfoxide; Dvl, Dishevelled; ER, endoplasmic reticulum; Fz3/Fz6, Frizzled 3/6; GFP, green fluorescent protein; HA, hemagglutinin; KS, Kolmogorov-Smirnov; NIH, National Institutes of Health; P0, postnatal day 0; PBS, phosphate-buffered saline; PCC, Pearson's correlation coefficient; PCP, planar cell polarity; Pk, Prickle; RFP, red fluorescent protein; ROI, region of interest; shRNA, short hairpin RNA; TGN, *trans*-Golgi network; Vangl1 and Vangl2, Van gogh-like 1 and 2; WGA, wheat germ agglutinin.

Wang *et al.*, 2005; Montcouquiol *et al.*, 2006; Chacon-Heszele *et al.*, 2012). In mutant animals carrying a loss-of-function allele of *Vangl2*, *Vangl2*$^{Lp/Lp}$ (Kibar *et al.*, 2001), core PCP proteins fail to correctly target the membrane in an asymmetrical manner, presumably underlying the loss of the coordinated orientation of sensory hair cells in those mutants (Curtin *et al.*, 2003; Montcouquiol *et al.*, 2003; Etheridge *et al.*, 2008). Despite the apparent essential role of polarized localization of core PCP proteins, the central question of the role of intracellular trafficking in the selective sorting and localization of core PCP proteins in vertebrates (Merte *et al.*, 2010; Wansleeben *et al.*, 2010) remains unclear.

Proteins destined for plasma membrane domains are processed along the biosynthetic pathway and segregated into distinct subsets of transport carriers emanating from the *trans*-Golgi network (TGN). Coat proteins mediate protein sorting at the TGN. Among known coat proteins, adaptor protein complexes play a major role in cargo selection and sorting/transport to regulate intercellular transport (Bonifacino, 2014; Park and Guo, 2014). In particular, recent studies show a potential role for adaptor proteins in the trafficking of membrane PCP proteins, for example, AP-1 in exporting Vangl2 from the TGN in cultured cells and in targeting Fz during establishment of PCP in *Drosophila* wing (Guo *et al.*, 2013; Carvajal-Gonzalez *et al.*, 2015) . There are five known AP complexes in the vertebrates, AP-1, AP-2, AP-3, AP-4, and AP-5. Each AP is composed of two large subunits (α, β, γ, δ, ε, or ζ), one medium subunit (μ1–μ5), and one small subunit (σ1–σ5) (Nakatsu *et al.*, 2014). Similar to small GTPase Rab proteins, AP complexes are localized to distinct but overlapping intracellular membranous compartments. AP-1, AP-3, and AP-4 are found at the TGN and endosomal membranes; AP-2 is localized to plasma membrane; and AP-5 is associated with late endosomes. Their localization denotes the trafficking events these APs regulate (Bonifacino, 2014; Park and Guo, 2014). AP complexes display specificity in membrane protein sorting by binding to selective sorting signals/motifs present in the cytoplasmic domain of membrane cargoes (Bonifacino and Traub, 2003; Bonifacino, 2014). Because adaptor selective localization and binding to sorting signals is required for the polarized partition of apical and basolateral proteins (Folsch, 2008), we asked whether adaptor-dependent sorting mechanisms segregate or regulate the subcellular localization of PCP membrane proteins along the polarity axis. We identified a novel interaction between AP-3 and Vangl2 in endosomal compartments and a requirement for AP-3 in Vangl2 membrane localization. We further took advantage of *AP-3* mutant mice carrying a null *mocha* allele of the large subunit delta adaptin of AP-3, *Ap3d1*$^{mh/mh}$, and identified PCP phenotypes in the organ of Corti that are associated with reduced membrane localization of Vangl2 and Fz3 and likely contribute to the auditory and vestibular dysfunctions we observed in the mutant mice. These results provide novel insight into the sorting pathways controlling PCP protein subcellular localization and reveal a novel role of the adaptor complex AP-3 in regulating PCP.

RESULTS

Vangl2 localizes to early and recycling endosomes

To explore PCP membrane protein–sorting endosomal pathways, we sought to identify cellular compartments where PCP proteins such as Vangl2 reside. We focused on adaptors and Rab proteins, which are small GTPases localizing to distinct membrane compartments within the endomembrane system (Schwartz *et al.*, 2007; Stenmark, 2009; Pfeffer, 2013; Wandinger-Ness and Zerial, 2014). We also tested pharmacological agents capable of disrupting trafficking in an organelle-selective manner.

We first examined the distribution of Vangl2 in IMCD3 cells transiently expressing GFP-Vangl2 relative to red fluorescent protein (RFP)-tagged endosomal Rab proteins, Rab4, Rab5, Rab11, and Rab21, by time-lapse microscopy (Bhuin and Roy, 2014). Whole-cell colocalization was quantified using Pearson's correlation coefficient (PCC), which quantifies how variations in two channels conform to each other irrespective of the gain (Newell-Litwa *et al.*, 2007; Blumer *et al.*, 2013; Tower-Gilchrist *et al.*, 2014). Vangl2 partially colocalized with Rab5-positive and Rab21-positive early endosomes (Figure 1, C and L), and with recycling endosome markers Rab4a and Rab11a (Figure 1, F and I). The overlap between early endosomes and Vangl2 had a PCC of 0.38, while the PCC between Vangl2 and recycling endosome Rab4a or Rab11a was 0.79–0.8 (Figure 1M). Not only was Vangl2 seen in the endosomal compartments, but it also was observed on the cell surface (Figure 1, A, D, G, and J). The colocalization of Vangl2 with recycling endosome Rab protein was also confirmed by using an antibody that recognizes the endogenous Rab11a in IMCD3 cells (Supplemental Figure S1).

Recycling Rab GTPases regulate membrane targeting (Bastin and Heximer, 2013). We used live-cell microscopy to further explore whether Vangl2 trafficks through the Rab4-recycling endosome pathway en route to the plasma membrane. Still images from real-time microscopy illustrated several events of Vangl2 sorting from Rab4 vesicles to the cell periphery (Figure 1N). A Vangl2-positive vesicle could be seen fusing with Rab4 endosomes at time zero, followed by budding off from the Rab4 endosome and moving to the plasma membrane (Figure 1N and Supplemental Movie 1). These events were observed at several locations in all of the 25 cells examined.

To further examine whether Vangl2 is targeted to the plasma membrane via recycling endosomes, we employed a pharmacological approach using LY294002, a known phosphoinositide 3-kinase inhibitor that inhibits transferrin recycling in recycling endosomes (van Dam *et al.*, 2002; Zhao and Keen, 2008) and in transporting cargoes to the cell membrane (Chen and Wang, 2001; Awwad *et al.*, 2007), to block aspects of Vangl2 sorting. As expected, cells treated with LY294002 contained enlarged Rab4 vesicles (Supplemental Figure S2, A–H), consistent with a disruption in recycling endocytic processes. Vangl2 membrane localization was observed in cells transiently expressing GFP-Vangl2 in the presence of dimethyl sulfoxide (DMSO) (Supplemental Figure S2, A, C, E, and G). However, in the presence of LY294002, Vangl2 membrane localization was reduced and Vangl2 was trapped in punctate intracellular structures of apparently aberrant endosomes (Supplemental Figure S2, B, D, and F). Furthermore, the dominant-negative form of Rab4a caused a similar reduction of Vangl2 membrane localization (Supplemental Figure S2, F and G). These data suggested that Vangl2 cycles through Rab4a-positive endosomal compartments.

Vangl2 interacts with adaptor protein-3 complex (AP-3)

We examined the association of Vangl2 with a coat protein known to localize to endosomes for which a viable mouse null mutant exists. The delta subunit of the coat protein complex adaptor protein-3 complex (AP-3) is mutated in the *mocha* mouse (*Ap3d1*$^{mh/mh}$) (Kantheti *et al.*, 1998). AP-3 localizes to early and recycling endosomes in diverse cell types (Peden *et al.*, 2004; Theos *et al.*, 2005; Newell-Litwa *et al.*, 2009). Following the finding that Vangl2 was present in endosomes and that a small fraction of Vangl2 colocalized with AP-3 (unpublished data), we tested whether AP-3 and Vangl2 proteins interact by coimmunoprecipitation (co-IP) (Figure 2). We detected a specific interaction between AP-3 and Vangl2 in cellular extracts (Figure 2A). The interaction between AP-3 and Vangl2

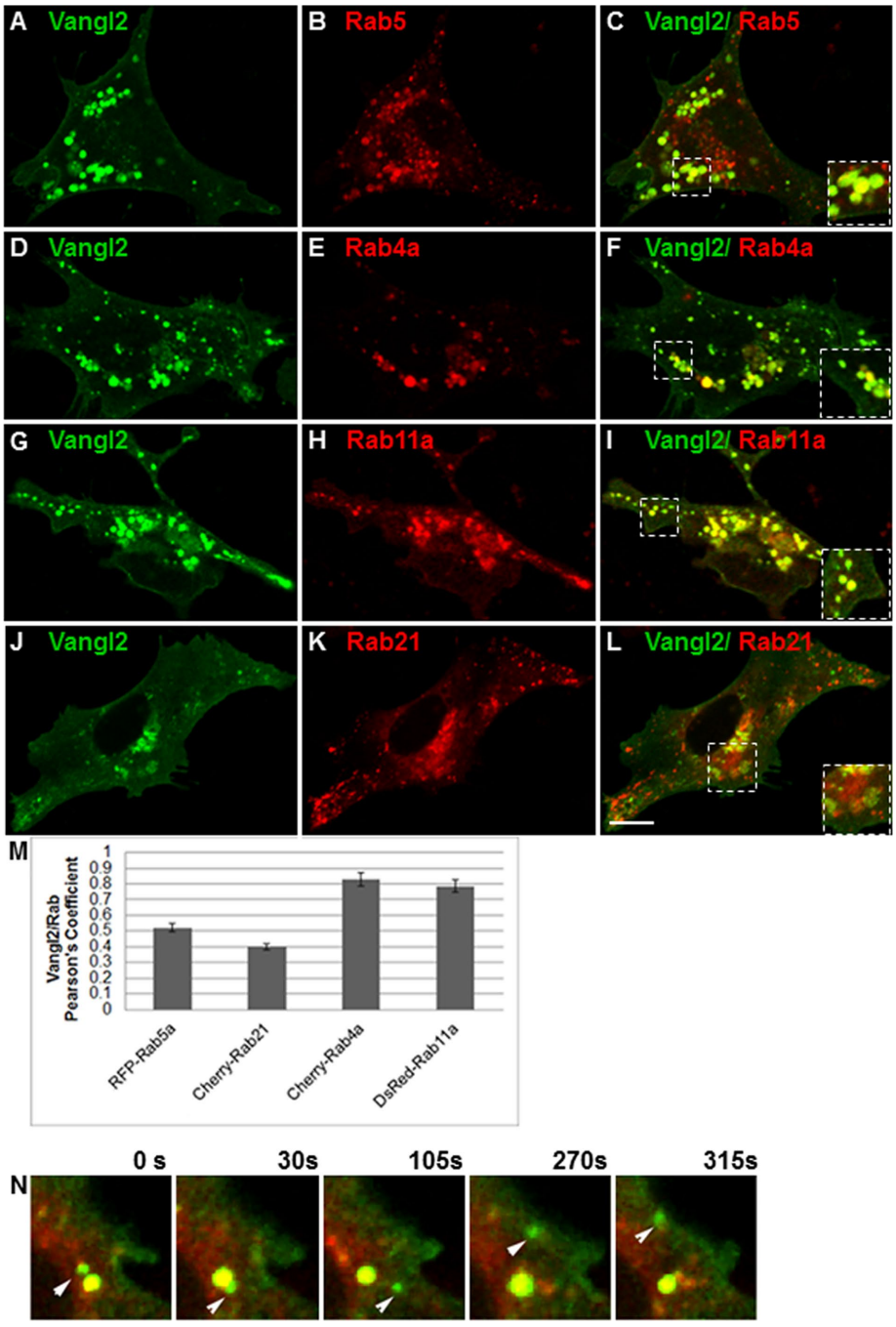

FIGURE 1: Vangl2 association with endocytic compartments. (A–L) IMCD3 cells were cotransfected with GFP-Vangl2 (green) and RFP-Rab5 (B), Cherry-Rab4a (E), DsRed-Rab11a (H), or Cherry-Rab21 (K). After 48 h, cells were imaged using time-lapse microscopy and a series of consecutive images were captured. A single frame from each series is shown (A–L). The white boxes mark the regions that were magnified in the corner of each panel to illustrate the colocalization of Vangl2 with each Rab protein. (M) Colocalization was quantified by PCCs of Vangl2 with each Rab. $N = 3$ transfections; 25 cells analyzed per condition. (N) Movement of GFP-Vangl2 vesicles from Rab4-positive endosomes toward the plasma membrane. IMCD3 cells were transfected with GFP-Vangl2 and Cherry-Rab4, cultured for 24 h, and then imaged live. Consecutive images were captured, and stills from the series at different times are shown. Scale bar: 19 μm.

was also detected using brain extracts isolated from animals expressing Vangl2–green fluorescent protein (Vangl2-GFP) protein (Figure 2B). The specificity of the co-IP by the AP-3 delta antibody was confirmed by immunoblotting with transferrin receptor, whose presence was only observed in the input (Figure 2A) and is known not to be associated with AP-3 (Dell'Angelica *et al.*, 1999; Newell-Litwa *et al.*, 2009). Moreover, to exclude any spurious interactions between Vangl2 and AP-3 antibody–coated beads, we outcompeted the binding of the AP-3 adaptor to its antibody using the AP-3 immunogenic delta peptide (Figure 2, A and B).

Depletion of the delta subunit of AP-3 causes loss of Vangl2 from the cell membrane

A functional interaction between AP-3 and Vangl2 predicts that Vangl2 subcellular distribution should be altered by AP-3 loss of function. Thus, we depleted AP-3 from cells using a short hairpin RNA (shRNA) against Ap3d1 (Figure 3 and Supplemental Figure S4) (Dong *et al.*, 2005). We used nonpermeabilized cells to directly detect Vangl2-GFP fluorescence and Alexa Fluor–labeled wheat germ agglutinin (WGA) to mark the cell surface. GFP-Vangl2 localized to the cell surface in most scrambled shRNA-infected cells (Figure 3, A–F′). In contrast, Vangl2 accumulated in perinuclear structures in 95% of the cells transfected with AP-3 shRNA (Figure 3, D–F, F′, H, and I, and Supplemental Figure S4). AP-3 shRNA did not affect the expression of Vangl2 (Figure 3G). These findings show that AP-3 is required for the membrane localization of Vangl2 in cultured cells. In addition, the influence of the loss of AP-3 on Vangl2 membrane localization was observed in varying confluent culture conditions (Figure 3 and Supplemental Figure S4), suggesting that cell–cell contacts may not be a requirement for Vangl2 membrane localization mediated by AP-3 in cultured cells.

Reduction of Vangl2 membrane localization in *AP-3*–deficient mice

Previous studies have reported postnatal hair cell loss in the organ of Corti in AP-3 delta 1 (*Ap3d1*)-deficient *mocha* animals (Lane and Deol, 1974; Rolfsen and Erway, 1984). However, it is not clear what the cellular defects are. Because AP-3 interacts with Vangl2 and is required for Vangl2 subcellular localization in cultured cells (Figures 3 and 4), we hypothesized that Vangl2 membrane localization may be disrupted and abnormal planar cell polarity may contribute to the overall defects observed in *Ap3d1*-deficient animals. To determine whether AP-3 has a role in Vangl2 trafficking in vivo, we bred animals carrying a Vangl2-GFP transgene (Qian *et al.*, 2007) with mice carrying an AP-3 functional null allele, $Ap3d1^{mh/mh}$ (Kantheti *et al.*, 1998) to obtain AP-3–deficient animals carrying the Vangl2-GFP transgene. The Vangl2-GFP transgenic animals carry two copies of the transgene that

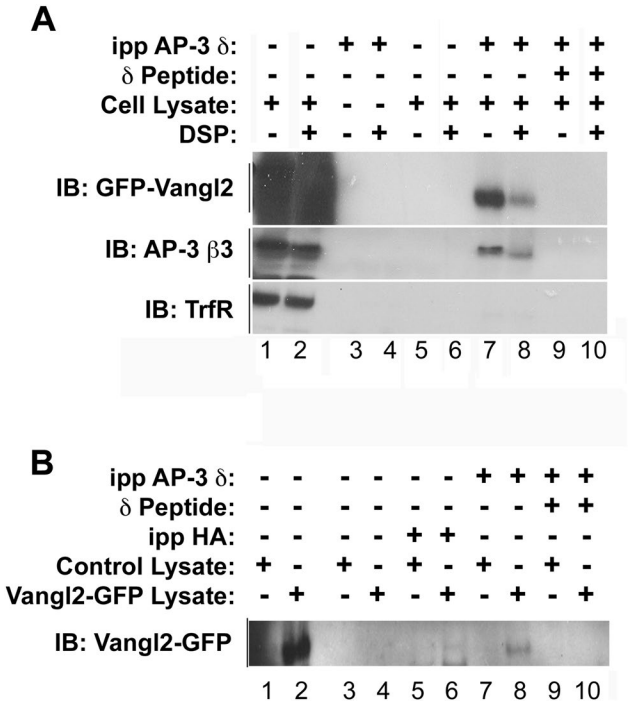

FIGURE 2: Vangl2 interacts with AP-3. (A) HEK293 cells were transiently transfected with GFP-Vangl2. Cell lysates were incubated at 4°C in the presence or absence of a cross-linker, DSP, and were immunoprecipitated with an anti–AP-3 SA4 delta antibody (A). Lanes 1 and 2 are input lanes (A,B). The resulting immune complexes were resolved by SDS–PAGE, and their compositions were assessed by immunoblot with antibodies against GFP, AP-3 beta, or transferrin receptor. Vangl2 was specifically pulled down by AP-3 antibody (lanes 7 and 8), and AP-3–specific peptide competition abolished the interaction between AP-3 and Vangl2 (lanes 9 and 10). (B) Brain protein extracts from neonatal control animals and animals expressing Vangl2-GFP were used for immunoprecipitations with an anti–AP-3 SA4 antibody. After incubation, the bound Vangl2 was detected by immunoblot using an anti-GFP antibody. AP-3 peptide competition abolished the interaction between AP-3 and Vangl2 (lanes 9 and 10). An antibody against HA served as an antibody control (lanes 5 and 6).

are under the control of Vangl2 regulatory elements and do not have any detectable cochlear or vestibular phenotypes (Qian *et al.*, 2007). The subcellular localization of Vangl2-GFP is identical to that of the endogenous Vangl2 observed (Montcouquiol *et al.*, 2006; Qian *et al.*, 2007; Belotti *et al.*, 2012), affording us a tool to examine Vangl2 localization in vivo.

Membrane or membrane-associated PCP proteins normally show a polarized membrane localization at cellular junctions in the cochlear epithelium at postnatal day 0 (P0), and disruption of the membrane localization of Vangl2 and other PCP proteins results in misorientation of sensory hair cells and cellular patterning defects from abnormal CE (Kibar *et al.*, 2001; Montcouquiol *et al.*, 2003; Wang *et al.*, 2005). As expected, Vangl2 appears on the apical cellular boundaries in control littermates (Figure 4, A, C, and E). In *Ap3d1*$^{mh/mh}$ animals, the plasma membrane levels of Vangl2 are drastically reduced across the length of the cochlear duct (Figure 4, B, D, and F), a phenotype reminiscent of the GFP-Vangl2 phenotypes observed in AP-3 down-regulated cells (Figure 3, D–F′).

We also performed antibody staining for Vangl2 and adherens junctional protein E-cadherin (Figure 4, G–J). We found a similar reduction of Vangl2 in *AP-3*–deficient mice (Figure 4, H and J) while the adherens junctional structure, revealed by staining for both E-cadherin and cortical F-actin associated with cellular junctional structures, appeared normal in *AP-3*–deficient mice (Figure 4, G and I). The loss or reduction of Vangl2 on the cell membrane in *AP-3*–deficient mice is likely to cause an alteration of PCP signaling, which will affect the polarized localization of other membrane or membrane-associated PCP proteins (Iliescu *et al.*, 2011). Furthermore, interactions between membrane PCP protein complexes at the cellular boundaries reinforce the polarized distribution of these proteins (Axelrod, 2009). We tested the possibility of AP-3 loss having an effect on other membrane PCP proteins. We evaluated the distribution of Fz3 in the cochlea at P0 (Figure 5). In control cochleae, Fz3 asymmetric staining is apparent and readily detectable at the cellular boundaries on the medial side of the hair cell membrane (Wang *et al.*, 2006a) (Figure 5, A–C). Confocal analysis of AP-3 mutant cochlea showed a reduction in Fz3 membrane localization (Figure 5, D–F). These results suggest that AP-3 is required for the membrane localization of Vangl2 at the apical cellular boundaries and that AP-3 deficiency influences Fz3 either directly or via the indirect effort of the loss of AP-3 on Vangl2 membrane targeting and PCP signaling.

AP-3 mutants exhibit characteristic PCP defects in the cochlea and are deaf

A morphogenetic readout for epithelial PCP in the cochlea is the formation of a precisely polarized hair bundle on the apical surface of each hair cell and coordinated polarity of all hair cells across the entire cochlea (Kelly and Chen, 2009). We further explored the hypothesis that *AP-3* deficiencies will have an effect on hair bundle morphology and orientation (Figure 6). In *AP-3*–deficient cochleae, there was a bundle misorientation phenotype as well as structural deformation of hair bundles where the hair bundles no longer formed a symmetric "V" shape (Figure 6, A–E). The hair bundles often appeared irregularly shaped, which was noticeable in the inner and outer third of hair cell rows in the organ of Corti of *AP-3* mutants but not of control animals (Figures 5 and 6, A–C and E). The kinocilium remained near the cortex of the V-shaped stereociliary bundle even in misoriented hair cells (Figure 5, G and J). We measured the hair bundle orientation and plotted the cumulative probability of the hair bundle orientation. We found that the difference in angle distribution between control and *AP-3*–deficient animals is statistically significant using the Kolmogorov-Smirnov (KS) test (Figure 6D). Similarly, we performed statistical analysis for the malformation of hair bundles using Student's *t* test and found that the difference between control and *AP-3*–deficient animals is significant (Figure 6E).

Examination of the cochleae at the onset of hearing showed that the general structure of the cochlea is maintained in *AP-3*–deficient animals (Supplemental Figure S3). Hair cell loss was evident in older animals (Supplemental Figure S3), consistent with a previous report (Rolfsen and Erway, 1984). We found that the *AP-3*–deficient animals are profoundly deaf (Supplemental Figure S6A), potentially caused by both defects in hair bundles and loss of hair cells.

The vertebrate PCP pathway regulates CE, a type of polarized cellular rearrangement that drives the tissue to converge along one axis and extend along a perpendicular axis (Wallingford *et al.*, 2001; Goto and Keller, 2002). In addition to regulating hair bundle morphology and orientation, essential vertebrate PCP genes also regulate CE in the terminally differentiating cochlea (Keller, 2002; Montcouquiol *et al.*, 2003; Torban *et al.*, 2004; Wang *et al.*, 2005). Defects in PCP signaling and defective CE lead to cellular patterning defects in the cochlea, including a shortened cochlea with additional rows of sensory hair cells in a widened sensory epithelium, known as the organ of Corti (Montcouquiol and Kelley, 2003; Wang *et al.*, 2005). In more than 60% of the *Ap3d1*$^{mh/mh}$ animals, we

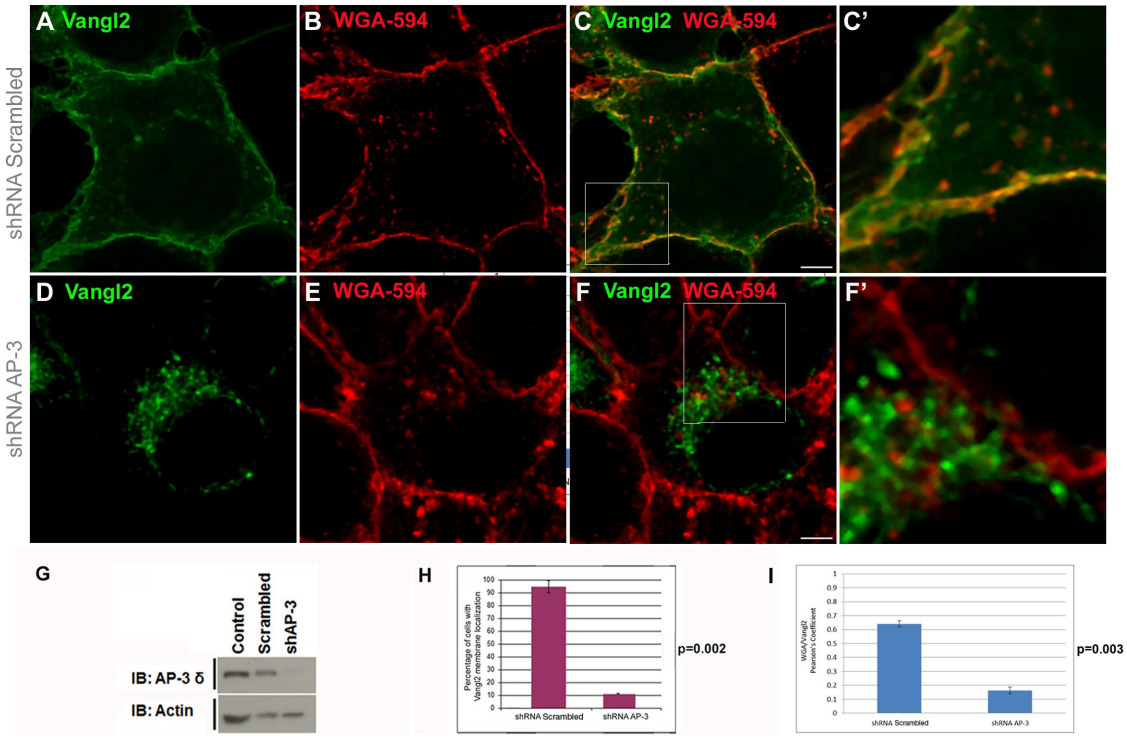

FIGURE 3: Knockdown of AP-3δ redistributes Vangl2 from the plasma membrane. HEK293 cells were infected with lentiviral shRNA against nontargeting shRNA (scrambled) (A–C, C′) or with shRNA against AP-3δ subunit (D–F, F′) for 72 h before puromycin selection was started. Cells were then transfected with GFP-Vangl2 for 48 h; this was followed by a quick staining with WGA-594 to mark cell membranes. Vangl2 was not detected on the membrane and was observed in punctuate structures throughout the cell in most cells depleted of AP-3δ. C′ and F′ are large views of the boxed regions in C and F, respectively. The cultures were confluent for both scrambled and AP-3 shRNA conditions. Cultures with less confluency (Supplemental Figure S4) showed similar results. (G) Cell lysates were collected and subjected to Western blot analysis of protein lysates using anti–AP-3δ SA4 antibody, revealing a reduction of > 95% in AP-3 levels by shRNA against AP-3. (F) The percent of Vangl2 redistribution in AP-3–depleted cells was quantified (H). The numbers of cells with Vangl2 on the membrane were significantly lower than that of controls. One hundred cells were counted per condition in each experimental set, and the experiments were repeated three times. Vangl2 membrane localization was quantified by measuring Pearson's coefficient of Vangl2 and WGA in shRNA Scrambled and shRNA AP-3 cells (I). $N = 3$; 50 cells analyzed. Scale bars: 19 μm. $p < 0.002$. Error bars represent SD.

observed extra rows of hair cells (Figure 6C). In addition, the cochlear duct was shorter in some of the *Ap3d1*$^{mh/mh}$ cochleae compared with the control cochleae (Figure 6F).

Together, the data (Figure 4) indicate that AP-3 is required for membrane localization of Vangl2 at the cellular boundaries in the cochlea. The reduction of Vangl2 membrane localization in *AP-3*–deficient mice likely contributes to the abnormality in hair cell patterning and hair bundle polarity (Figure 6, B–E). The morphological abnormality observed in stereociliary bundles (Figure 6) may be caused by additional cargoes of AP-3 that are essential for the formation of stereociliary bundles. AP-3 is an essential gene for cochlear development, maturation, and function (Figure 6 and Supplemental Figures S3 and S4).

AP-3 mutants have characteristic PCP defects in the vestibular sensory organ

Ap3d1$^{mh/mh}$ mice exhibited head tilt and circling behavior (Jones *et al.*, 2004). The underlying morphological and cellular defects, however, are not known. The tilted-head behavior in *AP-3*–deficient mice and the head bobbing observed in the *Vangl2 loop-tail* mutant animals (Strong and Hollander, 1949) are both consistent with vestibular abnormalities. We performed a number of behavioral tests to see whether the AP-3–deficient animals have additional behavior abnormalities indicative of a vestibular defect. We noticed that *Ap3d1*$^{mh/mh}$ mice performed poorly in walking assessments in comparison to littermate controls, while both *Ap3d1*$^{+/mh}$ animals and wild-type animals performed to the same normal capacity (Supplemental Figure S4B). In addition, *Ap3d1*$^{mh/mh}$ animals were unable to swim and had to be immediately rescued from drowning (Supplemental Figure S4C). These phenotypes are often associated with defects in the vestibule (Hoffman *et al.*, 2006; Zhao *et al.*, 2008).

Given the PCP defects in the cochlea in *AP-3*–deficient mice (Figure 6) and the vestibular behavioral abnormalities (Supplemental Figure S4), we performed morphological characterization of the vestibular organs from these animals to see whether there is similarly a PCP-related defect in the vestibule. In control animals, all the hair cells were oriented in the same direction in the posterior crista (Figure 7, B and D, arrows). In *Ap3d1*$^{mh/mh}$ animals, hair cells were oriented in various directions (Figure 7, B and D, arrows). Together, these data suggest that the loss of function of AP-3 leads to a PCP-dependent developmental defect in hair cell orientation in the posterior crista.

DISCUSSION

An essential feature of PCP signaling, the coordinated polarization of cells within the group, is achieved by membrane PCP protein

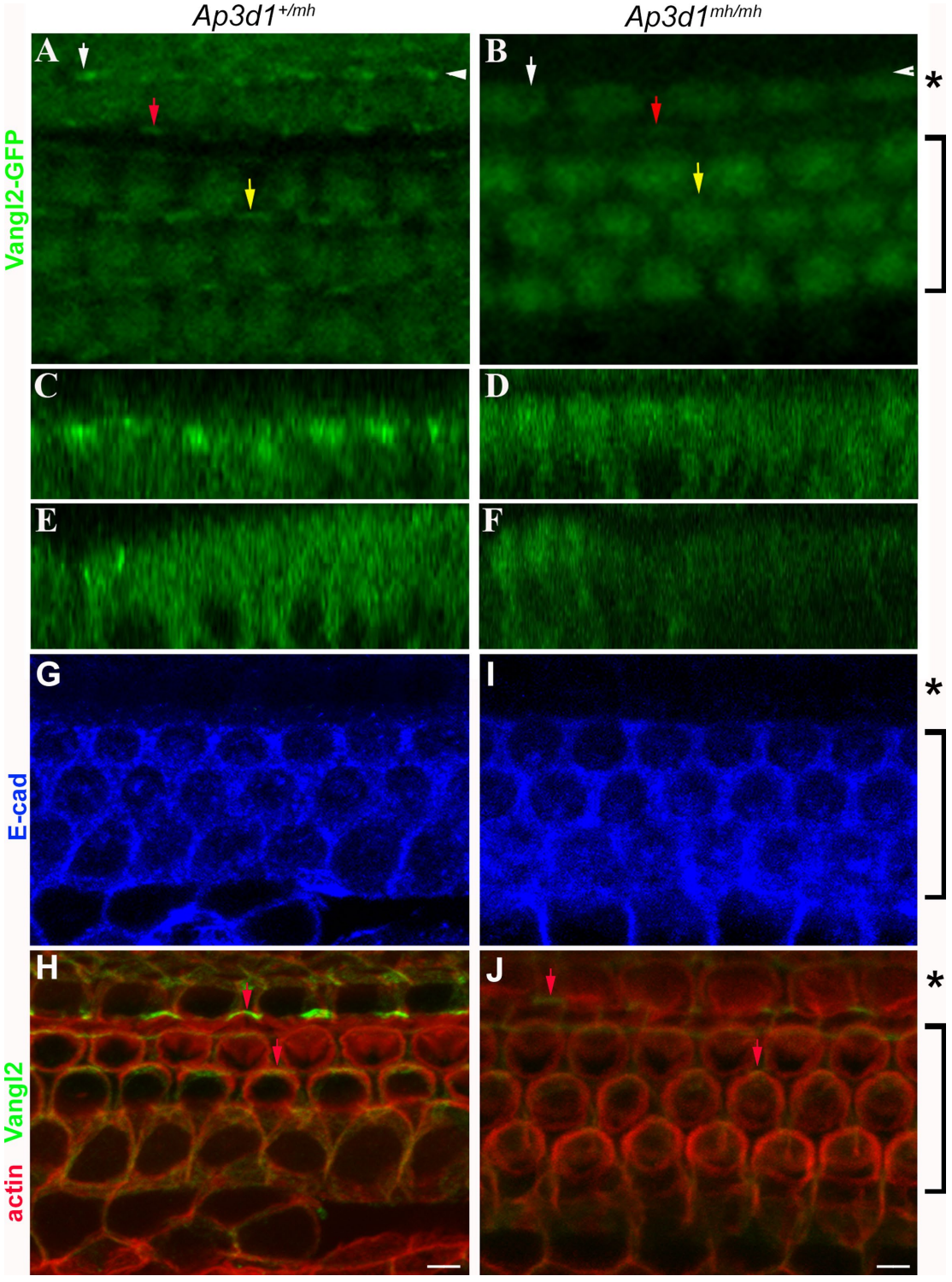

FIGURE 4: Disruption of Vangl2 membrane localization in *AP-3*–deficient cochlea. (A–F) Confocal images of cochlear whole mounts isolated at P0 from control mice (A, C, E) and *AP-3*–deficient *mocha* (*Ap3d1*$^{mh/mh}$) mice (B, D, F) expressing Vangl2-GFP. Vangl2-GFP signal at the cellular junctions was much reduced in homozygous *AP-3*–deficient *mocha* mutants (B), in comparison to the littermate controls (A). The orthogonal images of the confocal scans of the control (C, E) and *AP-3–deficient* (D, F) littermates indicated by the white arrowhead (C, D) and by the white arrow (E, F) were shown to visualize the distribution of Vangl2 protein throughout the cells. The red and yellow arrows mark Vangl2 membrane enrichment in comparable regions in the control (A) and AP-3 mutant (B) organ of Corti. Scale bars: 10 μm. (G–J) Confocal images of cochlear whole mounts isolated at P0 from control mice (G, H) and AP-3–deficient *mocha* (*Ap3d1*$^{mh/mh}$) mice (I, J) stained with antibodies against E-cadherin (blue) and Vangl2 (green) and phalloidin for F-actin (red). Note that Vangl2 asymmetric localization (indicated by arrows) was detected by the antibody against Vangl2, but the intensity of Vangl2 signaling in *Ap3d1*$^{mh/mh}$ mice was much reduced. The brackets mark the outer hair cell region, while the asterisks mark the inner hair cell region. E-cadherin showed a distinct boundary excluded from the inner hair cell region.

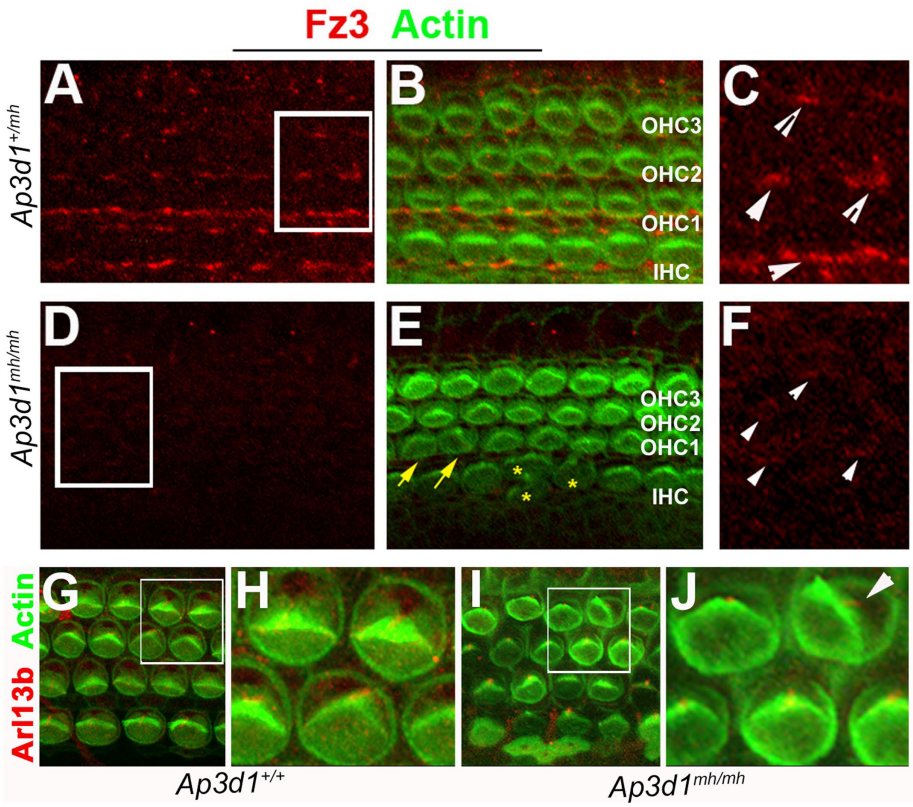

FIGURE 5: Distribution of Frizzled 3 in the organ of Corti of AP-3 deficient animals. (A–F) Immunostaining for Frizzled 3 (Fz3, red) in whole mounts of the organ of Corti at postnatal day 0 (P0) from basal regions of control (A–C) and *Ap3d1*$^{mh/mh}$ (D–F) cochleae. The level of Fz3 staining at the cell–cell junctional membranes is reduced in *Ap3d1*$^{mh/mh}$ mutants (D–F). Images in C and F are larger views of the boxed areas in A and D, respectively. The signal intensity of the boxed area (D) was enhanced (F) in order to illustrate the remaining junctional localizations of Fz3 in *Ap3d1*$^{mh/mh}$ mutants (arrowheads, F). Yellow arrows and asterisks (*) mark misoriented hair bundles and deformed hair bundles, respectively (E). IHC: inner hair cells; OHC1: outer hair cell row 1; OHC2: outer hair cell row 2; OHC3: outer hair cell row 3. (B, E). (G–J) Immunostaining for Arl13b (red), which visualizes the kinocilia, and F-actin (green) in whole mounts of the organ of Corti at postnatal day 0 (P0) from basal region of control (G, H) and *Ap3d1*$^{mh/mh}$ (I, J) cochleae. Images in H and J are larger views of the boxed areas in G and I, respectively. White arrowheads denote Fz3 localization. Note that the hair bundle morphology in *Ap3d1*$^{mh/mh}$ cochleae (I) appeared not as uniform as in control cochleae (G), and that the kinocilium remained at the vertex of the stereocilia bundle in normal and misoriented hair cells from *Ap3d1*$^{mh/mh}$ cochleae (I, J).

complexes formed at cellular boundaries asymmetrically in a polarized manner to mediate the polarity coordination between neighboring cells (Peng and Axelrod, 2012; Singh and Mlodzik, 2012). Limited studies have suggested the requirement of specific trafficking of core PCP components for establishment of PCP (Yu *et al.*, 2007; Mottola *et al.*, 2010; Strutt *et al.*, 2011). However, the network of trafficking machinery that contributes to the asymmetry distribution of membrane or membrane-associated PCP proteins is not clearly defined. Here, we showed that AP-3–dependent endosome traffic pathway is involved in membrane localization of Vangl2 in vitro and in vivo, supporting endosome traffic mechanisms in PCP regulation.

Vangl2 as a novel cargo of AP-3

Most membrane proteins are synthesized at the endoplasmic reticulum (ER), sorted by the COPII coating machinery into COPII vesicles, and exported from ER to the Golgi as the first trafficking event (Paczkowski *et al.*, 2015). After passage through the Golgi complex, proteins are packaged into vesicles that bud off the TGN and are delivered either to endosomal compartments or to the cell membrane (Yap and Winckler, 2015).

Two previous studies established the interaction between Vangl2 and Sec24b, a component of the COPII coat. (Merte *et al.*, 2010; Wansleeben *et al.*, 2010). In this study, we examined the role of endosome trafficking mechanisms in Vangl2 membrane localization. AP complexes play crucial roles in the transport of proteins to distinct cellular compartments within the endomembrane system, including sorting and assembling cargoes into endocytic vesicles at the TGN for membrane protein trafficking, by interactions through tyrosine- and dileucine-based sorting signals in the cytoplasmic tails of cargo proteins (Badolato and Parolini, 2007; Park and Guo, 2014). The AP-3 coat complex has been shown to function on endosomes and aid in trafficking of membrane proteins from endosomes (Peden *et al.*, 2004). A number of proteins have been identified as AP-3 cargoes, including TI-VAMP7 (Martinez-Arca *et al.*, 2003), CLC-3 and ZnT3 (Salazar *et al.*, 2004a, 2005a,b), phophatidylinositol-4-kinase type II α (Salazar *et al.*, 2004a, 2005b; Craige *et al.*, 2008), and tyrosinase (Theos *et al.*, 2005; Di Pietro *et al.*, 2006; Setty *et al.*, 2007; Sitaram *et al.*, 2012). Here, we propose that Vangl2 is a new AP-3 cargo. This model is supported by the coprecipitation of recombinant Vangl2 with endogenous AP-3, redistribution of Vangl2 away from the cell surface in AP-3–deplected cells in culture or in the cochlea from AP-3 mutant mice (Figures 2, 3, and 4), and phenotypes commonly associated with PCP mutants in *AP-3*–null cochleae and vestibules (Figures 5–7).

Roles of AP-3 in PCP protein membrane localization in vivo and in the formation and function of inner ear sensory organs

The mechanism of trafficking or sorting in the partition of PCP components has been explored by several recent studies. These studies identified a small repertoire of trafficking components such as Rabenosyn 5, Rab23, SEC24b, the adaptor complex AP-1, Arfaptin, and Arf1 (Mottola *et al.*, 2010; Pataki *et al.*, 2010; Wansleeben *et al.*, 2010; Guo *et al.*, 2013; Carvajal-Gonzalez *et al.*, 2015). Disruption in the protein trafficking pathways regulated by Sec24b or AP-1 leads to several PCP mutant phenotypes in vivo, including inner ear defects and failure of Vangl2 to reach cell membrane (Merte *et al.*, 2010; Wansleeben *et al.*, 2010). In particular, the studies of the role of AP-1 in PCP protein trafficking in *Drosophila* and zebrafish revealed loss of polarized distribution of Fz and Vang when AP-1 function is compromised (Carvajal-Gonzalez *et al.*, 2015). In this study, we found that membrane localization of Vangl2 is mediated by AP-3 endocytic

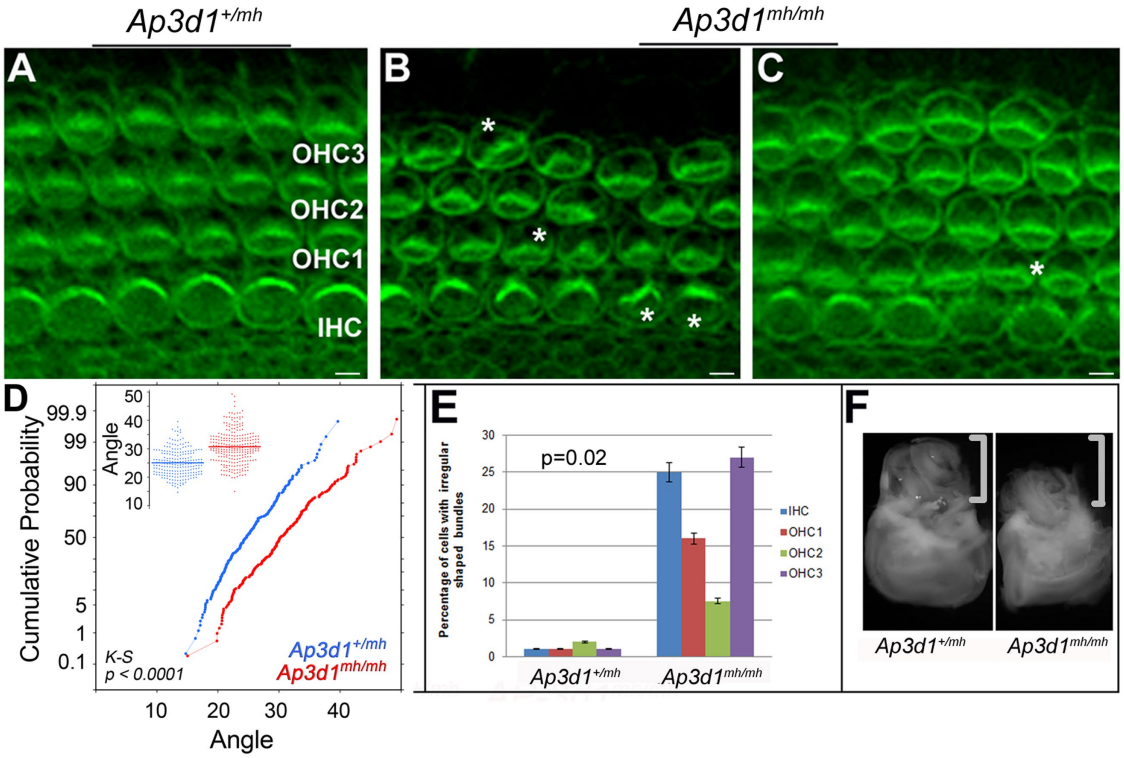

FIGURE 6: Polarity and patterning defects in *Ap3d1*$^{mh/mh}$ organ of Corti. (A–C) Cochleae at P0 from *Ap3d1*$^{+/mh}$ (A) and *Ap3d1*$^{mh/mh}$ (B, C) animals were stained for actin (phalloidin). The asterisks mark irregular hair bundles. IHC, inner hair cells; OHC1, outer hair cell row 1; OHC2, outer hair cell row 2; OHC3, outer hair cell row 3. Scale bars: 10 μm. (D, E). Quantification of OHC3 stereociliary bundle orientation from basal and medial regions of cochleae (D) and malformation of the bundles (E). We measured the orientation of hair bundles from *Ap3d1*$^{+/mh}$ and *Ap3d1*$^{mh/mh}$ animals and plotted the distribution of the angles (D, insert) and the cumulative probability of the angles (D). We also quantified the percentage of hair cells from the basal region of *Ap3d1*$^{+/mh}$ and *Ap3d1*$^{mh/mh}$ animals with abnormally flattened or deformed bundles (E). The statistical significance of the cumulative probability of angle distribution was performed using KS test (D). The statistic significance of the percentage of hair bundle malformation was performed using Student's *t* test (E). Data obtained from three animals per genotype. $p < 0.0001$ (bundle orientation); $p < 0.02$ (bundle morphology). (F) *Ap3d1*$^{mh/mh}$ animals have a smaller inner ear than control animals. The brackets mark the cochleae of inner ears in F.

pathways in cultured cells, as loss of AP-3 led to reduction of Vangl2 on the plasma membrane (Figure 3). We did note accumulation of Vangl2 into intracellular structures, and it would be important to further examine the destination of the missorted Vangl2. There a lack of overlap between Vangl2 with Rab4 and Rab5 in AP-3–depleted cells, which might suggest that Vangl2 is missorted away from the endosome (potentially into lysosomes) (unpublished data). Although we do not directly determine which pool of Vangl2 (newly synthesized or recycling) is being trafficked in this route, we provide evidence suggesting that the Rab4 endosome may play a role (Supplemental Figure S2). A study by Ma *et al*. (2018) demonstrates a distinct packaging of Vangl2 separate from Frizzled 6, events upstream of the endosomal pathway. Furthermore, the levels of Vangl2 on cellular junctions in the organ of Corti were greatly reduced in AP-3–deficient mice (Figure 4). This phenotype resembles another bona fide cargo, ZNT3, whose cellular content in neurons is reduced in AP-3 *mocha* animals (Kantheti *et al*., 1998; Salazar *et al*., 2004a,b). The results indicate AP-3 plays a role in Vangl2 membrane localization in vitro and in vivo.

Furthermore, we observed cochlear and vestibular morphological defects that are consistent with defective PCP signaling in *AP-3–deficient* mice (Figures 4–7) and may underlie the hearing and vestibular functional defects observed in such mice (Supplemental Figures S5 and S6). Previous studies show that *Ap3d1*$^{mh/mh}$ animals are deaf by testing hearing using the pinna response and report hair cell loss in older animals (Lane and Deol, 1974). In the vestibule, otoconial variations were seen in these animals (Rolfsen and Erway, 1984; Jones *et al*., 2004). In the current study, we found that the general structure of the cochlea is normal at onset of hearing, while the morphogenesis of the hair bundles and the patterning of the hair cells in the cochlea are affected in *AP-3*–deficient mice (Figure 6 and Supplemental Figure S3). The young *AP-3*–deficient animals are profoundly deaf, while littermates have normal hearing onset, as shown by auditory brainstem response (ABR) (Supplemental Figure S4). The PCP-like cellular defects likely contribute to the hearing defect in the cochlea. The loss of hair cells may be secondary to the loss of activity of hair cells, as hair cells remain in *Vglut3* mutant mice that are deaf (Ruel *et al*., 2008; Akil *et al*., 2012). A hair cell polarity defect was also observed in the vestibule (Figure 7), which may contribute to the functional defects in the vestibule (Supplemental Figure S4). In addition to a CE and hair bundle polarity abnormality in AP-3–deficient animals, there are also apparent abnormalities in hair bundle morphology (Figures 5–7).

The apical enrichment of an F-actin–associated protein appears to be abnormal in AP-3 mutants (Figure 7). It is possible that additional cargoes of AP-3 could contribute to the abnormal bundle

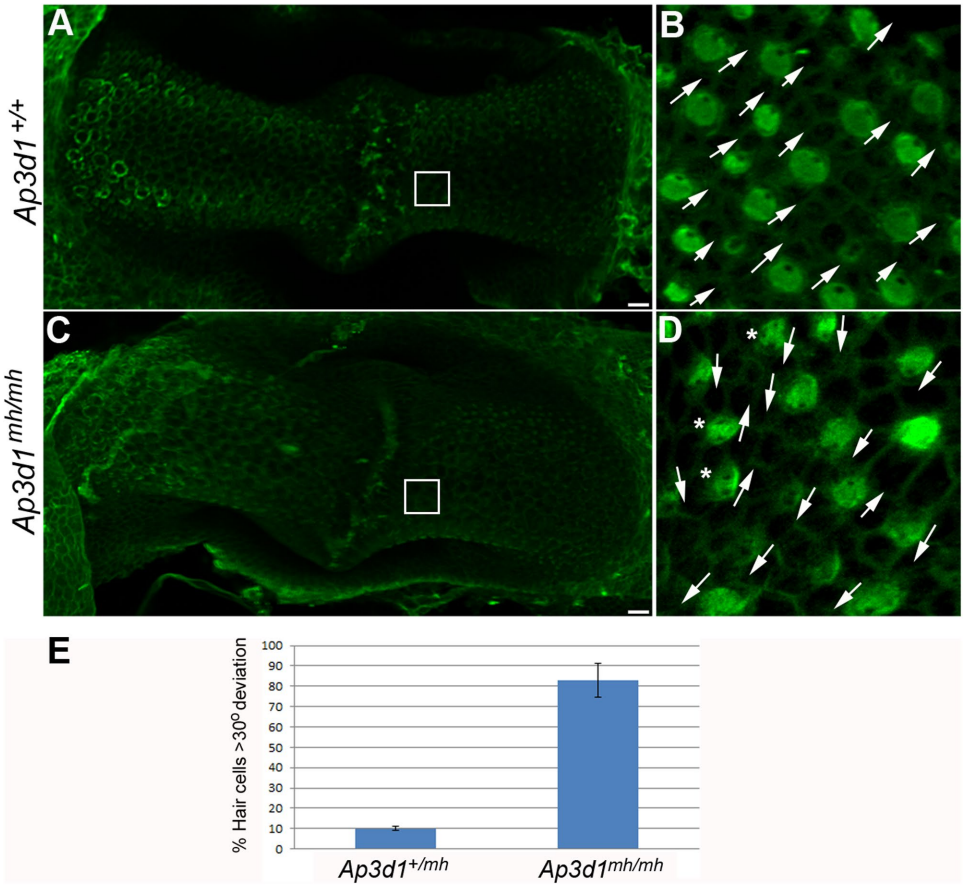

FIGURE 7: PCP defects in the posterior crista from *AP-3* mutant mice. Posterior crista from P0 control (A, B) and *Ap3d1*$^{mh/mh}$ (C, D) littermates were analyzed for hair cell orientation by staining with α-spectrin to visualize the position of the kinocilium (green). In *Ap3d1*$^{mh/mh}$ posterior crista, uniform hair cell orientation was disrupted and hair cells point in different directions (D, arrows) compared with the littermate control (B). The asterisks in D mark cells with spotty apical α-spectrin staining. Scale bars: 10 μm. (E) The misorientation of hair cells was quantified and plotted as described in *Materials and Methods*.

morphology and apical F-actin–associated protein enrichment. The published evidence suggests that apical-basal polarity can be established in cells lacking functional AP-3 complexes. Our results in neurons (Larimore *et al.*, 2011) and the data by Junking *et al.* (2014) in epithelial cells indicate that markers such as cadherins retain their polarized apical–basal distribution despite clear indications of defective AP-3–dependent cargo sorting. We have also observed normal E-cadherin localization in the cochlea in *AP-3* mutants (Figure 4). Moreover, ultrastructural studies of *AP-3*–null mouse kidney tubule cells indicate that there are no evident apical-basal polarity defects (Zhen *et al.*, 1999). These reports are consistent with our observations that cellular junctional structures, such as E-cadherin adherens junctions and cortical F-actin, appear normal in AP-3–deficient cochlea (Figure 4 and Supplemental Figure S4). Additional cargoes that are affected in AP-3–deficient mutants may regulate actin dynamics in hair bundle morphogenesis and the apical actin network in the cochlea.

MATERIALS AND METHODS

Mouse strains and animal care

Animal care and usage was in accordance with U.S. National Institutes of Health (NIH, Bethesda, MD) guidelines and was approved by the Animal Care and Use Committee of Emory University under the IACUC protocol no.: DAR-2001963-082815BN. The transgenic, Vangl2-GFP animals were generated as previously reported (Qian *et al.*, 2007). AP-3 mutant mice were purchased from Jackson Laboratories (stock no.: 000279, *gr* +/+ *Ap3d1*$^{mh/mh}$ *d*^{mh}/J) and are referred to as the *Ap3d1*^{mh} allele. The *Ap3d1*^{mh} allele is a functional null allele of *AP-3d1* (Kantheti *et al.*, 1998).

Antibodies and other reagents

The following antibodies and dyes were used in this study: affinity-purified anti-VAMP7 (a gift from Andrew Peden, Cambridge Institute for Research, Cambridge, UK); polyclonal anti–phosphatidylinositol-4-kianse type II α (PI4KIIα) (Guo *et al.*, 2003); monoclonal anti–AP-3 δ (SA4) (Developmental Studies Hybridoma Bank, University of Iowa, Iowa City, IA); polyclonal anti–AP-3 beta (cat. no. 13384-1-AP, Protein Tech Group, Chicago, IL); monoclonal anti–AP2 α-adaptin and anti-actin (cat. nos. A4325 and A5441, Sigma-Aldrich, St. Louis, MO); anti-hemagglutinin (HA; cat. no. A190108A, Bethyl Laboratories, Montgomery, TX); polyclonal anti-GFP (cat. no. 132002, Synaptic Systems, Goettingen, Germany); anti–α-spectrin (MAB1622, Chemicon); Rhodamine- or Alexa Fluor 488–conjugated phalloidin (Invitrogen); the antibody against Fz3 (a gift from J. Nathans, Johns Hopkins University, Baltimore, MD). Lipofectamine (cat. no. 11668-019) and puromycin (cat. no. 540411) were purchased from Invitrogen and Millipore, respectively. Anti-Vangl2 Clone 2G4 rat monoclonal antibody (gift from Jean-Paul Borg, INSERM-CNRS-Institut Paoli-Calmettes-Aix-Marseille Université, Marseille, France). Anti–E-cadherin monoclonal antibody was from BD Biosciences (cat. no. 610181, San Jose, CA). Anti-Rab11a rabbit antibody was from Cell Signaling (cat. no. 2413S, Danvers, MA). Anti-Rab4 and Rab5 antibodies were from Abcam (cat. nos. ab13252 and ab13253, Cambridge, MA). WGA, Alexa Fluor 594 conjugate was from ThermoFisher Scientific (cat. no. W11262, Grand Island, NY). LY294002 (cat. no. L9908-1MG) was from Sigma-Aldrich.

DNA constructs, oligonucleotides, and peptides

GFP-tagged Vangl2 (GFP-Vangl2) was obtained from Randy Schekman (University of California, Berkeley, CA). The pmCherry-C1-tagged Rab21 and pmCherry C2-Rab4aS22N were gifts from Elizabeth Sztul (University of Alabama at Birmingham, Birmingham, AL). pmCherry-C2-Rab4a wild-type was a gift from James Goldenring (Vanderbilt University Medical Center, Nashville, TN). DsRed-Rab11a wild-type (plasmid 12679) and mRFP-Rab5 wild-type plasmid (plasmid 14437) were from Addgene (Cambridge, MA) (Choudhury *et al.*, 2002; Sharma *et al.*, 2003; Vonderheit and Helenius, 2005). The oligonucleotides for AP-3δ (RHS4533-NM_003938) shRNA in a pLKO.1 vector for lentiviral infection were

obtained from Open Biosystems (Huntsville, AL) and used to silence expression of human AP-3. The scramble control shRNA in pLKO.1 was obtained from Addgene (vector 1864). The peptide of AP-3δ SA4 (AQQVDIVTEEMPENALPSDEDDKDPNDPYRA) (Salazar *et al.*, 2009) was purchased from Invitrogen (EvoQuest Team, Carlsbad, CA). The plasmid, μ2-HA-WT, was purchased from Addgene (plasmid 32752) (Nesterov *et al.*, 1999).

Cell cultures, transfections, and lentiviral infections

Mouse IMCD3s were grown in DMEM/Ham's F12 50/50 (cat. no. MT10092 CVRF, Invitrogen) mix with L-glutamine supplemented with 10% fetal bovine serum (cat. no. S11150, Atlanta Biologicals) and 100 U/ml penicillin/100 μg/ml streptomycin (cat. no. 15140122, Invitrogen) in a 37°C incubator with 5% CO_2. PC12 cells were cultured as previously described (Newell-Litwa *et al.*, 2007). Hek293T cells seeded in 35-mm plates were infected with 3 μl of lentivirus containing the shRNA constructs described earlier. After 24 h of being infected cells were incubated for up to 6 d in culture media supplemented with 4 μg/ml puromycin for selection as described in (Zlatic *et al.*, 2011). Hek293 cells were then transfected with lipofectamine 2000 (Invitrogen) with 2 μg of DNA for 48 h.

Immunoprecipitations and Western blot analysis

Standard methods were used for protein extraction and Western blotting (Craige *et al.*, 2008). Total protein concentrations were determined using the Bio-Rad protein assay (cat. no. 5000006). Proteins were separated by SDS–PAGE under reducing conditions and transferred onto a polyvinylidene difluoride (PVDF) membrane. Membranes were blocked in 5% dry milk and probed with specific primary antibodies and horseradish peroxidase–conjugated secondary antibodies.

Inner ear dissection, immunostaining, and imaging

Standard procedures were used for inner ear dissection, staining, and images (Jones and Chen, 2008). Inner ears were isolated with or without decalcification, fixed in 4% paraformaldehyde for 1 h either at room temperature or overnight at 4°C. The cochlear or vestibular epithelia were dissected and subjected to antibody staining as described previously (Wang *et al.*, 2006a; Ren *et al.*, 2013).

Time-lapse imaging was performed on a Nikon A1R confocal scope. Images were acquired for at least 15 s at 4 frames/s using NIS Elements (Nikon Instruments). Movies were then exported into Quicktime (Adobe Systems, San Jose, CA), and sequential still frames were taken from Quicktime movies. Localization and morphology images were captured using a Leica confocal imaging system. Further image analysis was done using Adobe Photoshop CS5.1 Extended, Image J (NIH), MetaMorph software (Sunnyvale, CA), or Volocity software programs. Confocal images were obtained using Nikon A1R, Olympus SzX12, Olympus FV1000/TIRF, or Zeiss LSM510.

For WGA, Alexa Fluor 594 labeling, cells were fixed in 4% paraformaldehyde for 15 min at room temperature; this was followed by three washes with Hank's balanced salt solution (HBSS). Cells were incubated with 5 μg/ml WGA diluted in phosphate-buffered saline (PBS) for 10 min at room temperature. Cells were then washed with HBSS two times and with PBS. Cells were permeabilized with 0.1% Triton X-100 in PBS for 7 min. The coverslips were then washed with PBS-T (PBS containing 0.2% Tween-20), and nuclei were stained with Hoechst for 5 min and washed with PBS before cells were mounted on slides.

ABR tests

Tone-burst ABR is an objective measurement of hearing thresholds at specific frequencies to detect hearing impairment sensitively. ABR tests were performed as previously described (Ahmad *et al.*, 2007; Chang *et al.*, 2015). Briefly, sound stimuli of particular frequencies from 4 to 32 kHz generated by the BioSig software package (Tucker-Davis Technologies, Alachua, FL) were delivered to anesthetized mice, and ABR responses were recorded and analyzed as previously described (Ahmad *et al.*, 2007).

Quantification of protein colocalization and morphology phenotype

We quantified colocalization using PCC, which quantifies how variations in two channels conform to each other irrespective of the gain. In-focus image planes were background subtracted with a 10-pixel rolling-ball algorithm in Fiji (ImageJ). A region of interest (ROI) immediately surrounding an individual cell was selected, and the Pearson coefficient was calculated by the Coloc 2 plug-in. Standard image rotation of 15° was used as a control to assess whether low colocalization values are just spurious channel overlap (Dunn *et al.*, 2011). In all the analyses, the whole cell was included in the ROI.

For quantification of the number of Rab4a-enlarged endosomes in DMSO- or LY294002-treated cells, endosome size was measured based on exogenous cherry-Rab4a expression and endogenous EEA1 staining. Each segmented endosome was marked as an ROI using the image segmentation tool in ImageJ that defines endosomes based on signal intensity. Size was measured for each ROI/endosome ($n = 30$) for each cell ($n = 25$). Endosomes falling in the 0.5- to 4.5-μm range were considered small compared with larger endosomes with sizes from 5 μm and up.

For determination of the V-shaped hair bundle orientation in the cochlea, a line was drawn from the position of the kinocilium through the middle of the V-shaped stereocilia (bisecting line). We defined the angle of orientation as the angle formed between the bisecting line and the line parallel to the medial to lateral axis of the cochlear duct. Normally, this angle is close to 0°. Each row of hair cells was divided into three groups according to its position along the longitudinal axis of the cochlea (base, middle, and apex) owing to the presence of a differentiation gradient within the cochlea during development. Hair cells from the base and middle regions were included for quantification, and hair cells from comparable regions within the cochleae were used for comparison among different genotypes. Hair cells in the apex region of the cochlear duct are less developed and not included for quantification. At least 25 hair cells were quantified for each sample at each region of the cochlea and at least 3 animals per genotype were analyzed.

To quantify hair cell orientation in the posterior crista, we measured hair cell orientation throughout the length of the cristae with the use of alpha-Spectrin staining to highlight the position of the fonticulus, or the bare region devoid of F-actin and alpha-Spectrin. Orientation differences between neighboring cells were observed in four quadrants. Angle deviations of 30° from the axis perpendicular to the long axis of the crista were considered misoriented. The tissues may be stretched during mounting, and the long axis was adjusted to correct the twist caused by stretching. The cells in each quadrant with misorientation were counted and recorded. The data from 3 cristae per genotype were averaged and plotted.

Statistics

A KS comparison was used to test statistical significance of the cumulative probability of hair bundle angle distributions between control and mutant animals using the engine www.physics.csbsju.edu/stats/KS-test.n.plot_form.html or the software package StatPlus Mac Built 5.6.0pre/Universal (AnalystSoft). A p value < 0.05 is considered to be significant. For the percentage of malformed hair

bundles in the control and mutant animals, the data are presented as average ± SD. Student's *t* tests were used to determine statistical significance of data obtained from control and mutant animals. A p value < 0.05 is considered significant.

ACKNOWLEDGMENTS

The pmCherry-C1-tagged Rab21 and pmCherry C2-Rab4aS22N were gifts from Elizabeth Sztul (University of Alabama at Birmingham, Birmingham, AL). pmCherry-C2-Rab4a wild-type was a gift from James Goldenring (Vanderbilt University Medical Center, Nashville, TN). Anti-Vangl2 Clone 2G4 rat monoclonal antibody was a gift from Jean-Paul Borg (INSERM-CNRS-Institut Paoli-Calmettes-Aix-Marseille Université, Marseille, France). This research project was supported by NIH grants ROI DC005213 to P.C., F32 DC0127 02 to C.T.-G., and GM077569 and CHOA for V.F. and S.A.Z. This research was also supported in part by the Emory University Integrated Cellular Imaging Microscopy Core.

REFERENCES

Ahmad S, Tang W, Chang Q, Qu Y, Hibshman J, Li Y, Sohl G, Willecke K, Chen P, Lin X (2007). Restoration of connexin26 protein level in the cochlea completely rescues hearing in a mouse model of human connexin30-linked deafness. Proc Natl Acad Sci USA 104, 1337–1341.

Akil O, Seal RP, Burke K, Wang C, Alemi A, During M, Edwards RH, Lustig LR (2012). Restoration of hearing in the VGLUT3 knockout mouse using virally mediated gene therapy. Neuron 75, 283–293.

Awwad HO, Iyer V, Rosenfeld JL, Millman EE, Foster E, Moore RH, Knoll BJ. (2007). Inhibitors of phosphoinositide 3-kinase cause defects in the postendocytic sorting of beta2-adrenergic receptors. Exp Cell Res 313, 2586–2596.

Axelrod JD (2009). Progress and challenges in understanding planar cell polarity signaling. Semin Cell Dev Biol 20, 964–971.

Badolato R, Parolini S (2007). Novel insights from adaptor protein 3 complex deficiency. J Allergy Clin Immunol 120, 735–741; quiz 742–733.

Bastin G, Heximer SP (2013). Rab family proteins regulate the endosomal trafficking and function of RGS4. J Biol Chem 288, 21836–21849.

Belotti E, Puvirajesinghe TM, Audebert S, Baudelet E, Camoin L, Pierres M, Lasvaux L, Ferracci G, Montcouquiol M, Borg JP (2012). Molecular characterisation of endogenous Vangl2/Vangl1 heteromeric protein complexes. PLoS One 7, e46213.

Bhuin T, Roy JK (2014). Rab proteins: the key regulators of intracellular vesicle transport. Exp Cell Res 328, 1–19.

Blumer J, Rey J, Dehmelt L, Mazel T, Wu YW, Bastiaens P, Goody RS, Itzen A (2013). RabGEFs are a major determinant for specific Rab membrane targeting. J Cell Biol 200, 287–300.

Bonifacino JS (2014). Adaptor proteins involved in polarized sorting. J Cell Biol 204, 7–17.

Bonifacino JS, Traub LM (2003). Signals for sorting of transmembrane proteins to endosomes and lysosomes. Annu Rev Biochem 72, 395–447.

Carvajal-Gonzalez JM, Balmer S, Mendoza M, Dussert A, Collu G, Roman AC, Weber U, Ciruna B, Mlodzik M (2015). The clathrin adaptor AP-1 complex and Arf1 regulate planar cell polarity in vivo. Nat Commun 6, 6751.

Chacon-Heszele MF, Ren D, Reynolds AB, Chi F, Chen P (2012). Regulation of cochlear convergent extension by the vertebrate planar cell polarity pathway is dependent on p120-catenin. Development 139, 968–978.

Chang Q, Wang J, Li Q, Kim Y, Zhou B, Wang Y, Li H, Lin X (2015). Virally mediated Kcnq1 gene replacement therapy in the immature scala media restores hearing in a mouse model of human Jervell and Lange-Nielsen deafness syndrome. EMBO Mol Med 7, 1077–1086.

Chen X, Wang Z (2001). Regulation of epidermal growth factor receptor endocytosis by wortmannin through activation of Rab5 rather than inhibition of phosphatidylinositol 3-kinase. EMBO Rep 2, 842–849.

Choudhury A, Dominguez M, Puri V, Sharma DK, Narita K, Wheatley CL, Marks DL, Pagano RE (2002). Rab proteins mediate Golgi transport of caveola-internalized glycosphingolipids and correct lipid trafficking in Niemann-Pick C cells. J Clin Invest 109, 1541–1550.

Craige B, Salazar G, Faundez V (2008). Phosphatidylinositol-4-kinase type II alpha contains an AP-3-sorting motif and a kinase domain that are both required for endosome traffic. Mol Biol Cell 19, 1415–1426.

Curtin JA, Quint E, Tsipouri V, Arkell RM, Cattanach B, Copp AJ, Henderson DJ, Spurr N, Stanier P, Fisher EM, *et al.* (2003). Mutation of Celsr1 disrupts planar polarity of inner ear hair cells and causes severe neural tube defects in the mouse. Curr Biol 13, 1129–1133.

Dell'Angelica EC, Shotelersuk V, Aguilar RC, Gahl WA, Bonifacino JS (1999). Altered trafficking of lysosomal proteins in Hermansky-Pudlak syndrome due to mutations in the beta 3A subunit of the AP-3 adaptor. Mol Cell 3, 11–21.

Di Pietro SM, Falcon-Perez JM, Tenza D, Setty SR, Marks MS, Raposo G, Dell'Angelica EC (2006). BLOC-1 interacts with BLOC-2 and the AP-3 complex to facilitate protein trafficking on endosomes. Mol Biol Cell 17, 4027–4038.

Dong X, Li H, Derdowski A, Ding L, Burnett A, Chen X, Peters TR, Dermody TS, Woodruff E, Wang JJ, *et al.* (2005). AP-3 directs the intracellular trafficking of HIV-1 Gag and plays a key role in particle assembly. Cell 120, 663–674.

Dunn KW, Kamocka MM, McDonald JH (2011). A practical guide to evaluating colocalization in biological microscopy. Am J Physiol Cell Physiol 300, C723–C742.

Etheridge SL, Ray S, Li S, Hamblet NS, Lijam N, Tsang M, Greer J, Kardos N, Wang J, Sussman DJ, *et al.* (2008). Murine dishevelled 3 functions in redundant pathways with dishevelled 1 and 2 in normal cardiac outflow tract, cochlea, and neural tube development. PLoS Genet 4, e1000259.

Folsch H (2008). Regulation of membrane trafficking in polarized epithelial cells. Curr Opin Cell Biol 20, 208–213.

Goto T, Keller R (2002). The planar cell polarity gene strabismus regulates convergence and extension and neural fold closure in *Xenopus*. Dev Biol 247, 165–181.

Guo J, Wenk MR, Pellegrini L, Onofri F, Benfenati F, De Camilli P (2003). Phosphatidylinositol 4-kinase type IIα is responsible for the phosphatidylinositol 4-kinase activity associated with synaptic vesicles. Proc Natl Acad Sci USA 100, 3995–4000.

Guo N, Hawkins C, Nathans J (2004). Frizzled6 controls hair patterning in mice. Proc Natl Acad Sci USA 101, 9277–9281.

Guo Y, Zanetti G, Schekman R (2013). A novel GTP-binding protein-adaptor protein complex responsible for export of Vangl2 from the *trans* Golgi network. Elife 2, e00160.

Hoffman LF, Ross MD, Varelas J, Jones SM, Jones TA (2006). Afferent synapses are present in utricular hair cells from otoconia-deficient mice. Hear Res 222, 35–42.

Iliescu A, Gravel M, Horth C, Kibar Z, Gros P (2011). Loss of membrane targeting of Vangl proteins causes neural tube defects. Biochemistry 50, 795–804.

Jones C, Chen P (2008). Primary cilia in planar cell polarity regulation of the inner ear. Curr Top Dev Biol 85, 197–224.

Jones SM, Erway LC, Johnson KR, Yu H, Jones TA (2004). Gravity receptor function in mice with graded otoconial deficiencies. Hear Res 191, 34–40.

Junking M, Sawasdee N, Duangtum N, Cheunsuchon B, Limjindaporn T, Yenchitsomanus PT (2014). Role of adaptor proteins and clathrin in the trafficking of human kidney anion exchanger 1 (kAE1) to the cell surface. Traffic 15, 788–802.

Kantheti P, Qiao X, Diaz ME, Peden AA, Meyer GE, Carskadon SL, Kapfhamer D, Sufalko D, Robinson MS, Noebels JL, *et al.* (1998). Mutation in AP-3 delta in the mocha mouse links endosomal transport to storage deficiency in platelets, melanosomes, and synaptic vesicles. Neuron 21, 111–122.

Keller R (2002). Shaping the vertebrate body plan by polarized embryonic cell movements. Science 298, 1950–1954.

Kelly MC, Chen P (2009). Development of form and function in the mammalian cochlea. Curr Opin Neurobiol 19, 395–401.

Kibar Z, Vogan KJ, Groulx N, Justice MJ, Underhill DA, Gros P (2001). Ltap, a mammalian homolog of *Drosophila* Strabismus/Van Gogh, is altered in the mouse neural tube mutant Loop-tail. Nat Genet 28, 251–255.

Lane PW, Deol MS (1974). Mocha, a new coat color and behavior mutation on chromosome 10 of the mouse. J Hered 65, 362–364.

Larimore J, Tornieri K, Ryder PV, Gokhale A, Zlatic SA, Craige B, Lee JD, Talbot K, Pare JF, Smith Y, *et al.* (2011). The schizophrenia susceptibility factor dysbindin and its associated complex sort cargoes from cell bodies to the synapse. Mol Biol Cell 22, 4854–4867.

Ma T, Li B, Wang R, Lau PK, Huang Y, Jiang L, Schekman R, Guo Y (2018). A mechanism for differential sorting of the planar cell polarity proteins Frizzled6 and Vangl2 at the trans-Golgi network. J Biol Chem 293, 8410–8427.

Martinez-Arca S, Rudge R, Vacca M, Raposo G, Camonis J, Proux-Gillardeaux V, Daviet L, Formstecher E, Hamburger A, Filippini F, *et al.* (2003). A

dual mechanism controlling the localization and function of exocytic v-SNAREs. Proc Natl Acad Sci USA 100, 9011–9016.
McNeill H (2010). Planar cell polarity: keeping hairs straight is not so simple. Cold Spring Harb Perspect Biol 2, a003376.
Merte J, Jensen D, Wright K, Sarsfield S, Wang Y, Schekman R, Ginty DD (2010). Sec24b selectively sorts Vangl2 to regulate planar cell polarity during neural tube closure. Nat Cell Biol 12, 41–46; sup pp 1–8.
Montcouquiol M, Jones JM, Sans N (2008). Detection of planar polarity proteins in mammalian cochlea. Methods Mol Biol 468, 207–219.
Montcouquiol M, Kelley MW (2003). Planar and vertical signals control cellular differentiation and patterning in the mammalian cochlea. J Neurosci 23, 9469–9478.
Montcouquiol M, Rachel RA, Lanford PJ, Copeland NG, Jenkins NA, Kelley MW (2003). Identification of Vangl2 and Scrb1 as planar polarity genes in mammals. Nature 423, 173–177.
Montcouquiol M, Sans N, Huss D, Kach J, Dickman JD, Forge A, Rachel RA, Copeland NG, Jenkins NA, Bogani D, *et al.* (2006). Asymmetric localization of Vangl2 and Fz3 indicate novel mechanisms for planar cell polarity in mammals. J Neurosci 26, 5265–5275.
Mottola G, Classen AK, Gonzalez-Gaitan M, Eaton S, Zerial M (2010). A novel function for the Rab5 effector Rabenosyn-5 in planar cell polarity. Development 137, 2353–2364.
Nakatsu F, Hase K, Ohno H (2014). The role of the clathrin adaptor AP-1: polarized sorting and beyond. Membranes 4, 747–763.
Nesterov A, Carter RE, Sorkina T, Gill GN, Sorkin A (1999). Inhibition of the receptor-binding function of clathrin adaptor protein AP-2 by dominant-negative mutant mu2 subunit and its effects on endocytosis. EMBO J 18, 2489–2499.
Newell-Litwa K, Salazar G, Smith Y, Faundez V (2009). Roles of BLOC-1 and adaptor protein-3 complexes in cargo sorting to synaptic vesicles. Mol Biol Cell 20, 1441–1453.
Newell-Litwa K, Seong E, Burmeister M, Faundez V (2007). Neuronal and non-neuronal functions of the AP-3 sorting machinery. J Cell Sci 120, 531–541.
Paczkowski JE, Richardson BC, Fromme JC (2015). Cargo adaptors: structures illuminate mechanisms regulating vesicle biogenesis. Trends Cell Biol 25, 408–416.
Park SY, Guo X (2014). Adaptor protein complexes and intracellular transport. Biosci Rep 34, e00123.
Park TJ, Haigo SL, Wallingford JB (2006). Ciliogenesis defects in embryos lacking inturned or fuzzy function are associated with failure of planar cell polarity and Hedgehog signaling. Nat Genet 38, 303–311.
Pataki C, Matusek T, Kurucz E, Ando I, Jenny A, Mihaly J (2010). *Drosophila* Rab23 is involved in the regulation of the number and planar polarization of the adult cuticular hairs. Genetics 184, 1051–1065.
Peden AA, Oorschot V, Hesser BA, Austin CD, Scheller RH, Klumperman J (2004). Localization of the AP-3 adaptor complex defines a novel endosomal exit site for lysosomal membrane proteins. J Cell Biol 164, 1065–1076.
Peng Y, Axelrod JD (2012). Asymmetric protein localization in planar cell polarity: mechanisms, puzzles, and challenges. Curr Top Dev Biol 101, 33–53.
Pfeffer SR (2013). Rab GTPase regulation of membrane identity. Curr Opin Cell Biol 25, 414–419.
Qian D, Jones C, Rzadzinska A, Mark S, Zhang X, Steel KP, Dai X, Chen P (2007). Wnt5a functions in planar cell polarity regulation in mice. Dev Biol 306, 121–133.
Ren DD, Kelly M, Kim SM, Grimsley-Myers CM, Chi FL, Chen P (2013). Testin interacts with vangl2 genetically to regulate inner ear sensory cell orientation and the normal development of the female reproductive tract in mice. Dev Dyn 242, 1454–1465.
Rolfsen RM, Erway LC (1984). Trace metals and otolith defects in mocha mice. J Hered 75, 159–162.
Ruel J, Emery S, Nouvian R, Bersot T, Amilhon B, Van Rybroek JM, Rebillard G, Lenoir M, Eybalin M, Delprat B, *et al.* (2008). Impairment of SLC17A8 encoding vesicular glutamate transporter-3, VGLUT3, underlies nonsyndromic deafness DFNA25 and inner hair cell dysfunction in null mice. Am J Hum Genet 83, 278–292.
Salazar G, Craige B, Love R, Kalman D, Faundez V (2005a). Vglut1 and ZnT3 co-targeting mechanisms regulate vesicular zinc stores in PC12 cells. J Cell Sci 118, 1911–1921.
Salazar G, Craige B, Wainer BH, Guo J, De Camilli P, Faundez V (2005b). Phosphatidylinositol-4-kinase type II alpha is a component of adaptor protein-3-derived vesicles. Mol Biol Cell 16, 3692–3704.
Salazar G, Love R, Styers ML, Werner E, Peden A, Rodriguez S, Gearing M, Wainer BH, Faundez V (2004a). AP-3-dependent mechanisms control the targeting of a chloride channel (ClC-3) in neuronal and non-neuronal cells. J Biol Chem 279, 25430–25439.
Salazar G, Love R, Werner E, Doucette MM, Cheng S, Levey A, Faundez V (2004b). The zinc transporter ZnT3 interacts with AP-3 and it is preferentially targeted to a distinct synaptic vesicle subpopulation. Mol Biol Cell 15, 575–587.
Salazar G, Zlatic S, Craige B, Peden AA, Pohl J, Faundez V (2009). Hermansky-Pudlak syndrome protein complexes associate with phosphatidylinositol 4-kinase type II alpha in neuronal and non-neuronal cells. J Biol Chem 284, 1790–1802.
Schwartz SL, Cao C, Pylypenko O, Rak A, Wandinger-Ness A (2007). Rab GTPases at a glance. J Cell Sci 120, 3905–3910.
Setty SR, Tenza D, Truschel ST, Chou E, Sviderskaya EV, Theos AC, Lamoreux ML, Di Pietro SM, Starcevic M, Bennett DC, *et al.* (2007). BLOC-1 is required for cargo-specific sorting from vacuolar early endosomes toward lysosome-related organelles. Mol Biol Cell 18, 768–780.
Sharma DK, Choudhury A, Singh RD, Wheatley CL, Marks DL, Pagano RE (2003). Glycosphingolipids internalized via caveolar-related endocytosis rapidly merge with the clathrin pathway in early endosomes and form microdomains for recycling. J Biol Chem 278, 7564–7572.
Singh J, Mlodzik M (2012). Planar cell polarity signaling: coordination of cellular orientation across tissues. Wiley Interdiscip Rev Dev Biol 1, 479–499.
Sitaram A, Dennis MK, Chaudhuri R, De Jesus-Rojas W, Tenza D, Setty SR, Wood CS, Sviderskaya EV, Bennett DC, Raposo G, *et al.* (2012). Differential recognition of a dileucine-based sorting signal by AP-1 and AP-3 reveals a requirement for both BLOC-1 and AP-3 in delivery of OCA2 to melanosomes. Mol Biol Cell 23, 3178–3192.
Stenmark H (2009). Rab GTPases as coordinators of vesicle traffic. Nat Rev Mol Cell Biol 10, 513–525.
Strong LC, Hollander WF (1949). Hereditary loop-tail in the house mouse—accompanied by imperforate vagina and with lethal craniorachischisis when homozygous. J Hered 40, 329–334.
Strutt H, Warrington SJ, Strutt D (2011). Dynamics of core planar polarity protein turnover and stable assembly into discrete membrane subdomains. Dev Cell 20, 511–525.
Theos AC, Tenza D, Martina JA, Hurbain I, Peden AA, Sviderskaya EV, Stewart A, Robinson MS, Bennett DC, Cutler DF, *et al.* (2005). Functions of adaptor protein (AP)-3 and AP-1 in tyrosinase sorting from endosomes to melanosomes. Mol Biol Cell 16, 5356–5372.
Torban E, Kor C, Gros P (2004). Van Gogh-like2 (Strabismus) and its role in planar cell polarity and convergent extension in vertebrates. Trends Genet 20, 570–577.
Tower-Gilchrist C, Styers ML, Yoder BK, Berbari NF, Sztul E (2014). Monitoring endosomal trafficking of the g protein-coupled receptor somatostatin receptor 3. Methods Enzymol 534, 261–280.
van Dam EM, Ten Broeke T, Jansen K, Spijkers P, Stoorvogel W (2002). Endocytosed transferrin receptors recycle via distinct dynamin and phosphatidylinositol 3-kinase-dependent pathways. J Biol Chem 277, 48876–48883.
Veeman MT, Axelrod JD, Moon RT (2003). A second canon. Functions and mechanisms of beta-catenin-independent Wnt signaling. Dev Cell 5, 367–377.
Vonderheit A, Helenius A (2005). Rab7 associates with early endosomes to mediate sorting and transport of Semliki Forest virus to late endosomes. PLoS Biol 3, e233.
Wallingford JB, Harland RM (2002). Neural tube closure requires Dishevelled-dependent convergent extension of the midline. Development 129, 5815–5825.
Wallingford JB, Vogeli KM, Harland RM (2001). Regulation of convergent extension in *Xenopus* by Wnt5a and Frizzled-8 is independent of the canonical Wnt pathway. Int J Dev Biol 45, 225–227.
Wandinger-Ness A, Zerial M (2014). Rab proteins and the compartmentalization of the endosomal system. Cold Spring Harb Perspect Biol 6, a022616.
Wang J, Hamblet NS, Mark S, Dickinson ME, Brinkman BC, Segil N, Fraser SE, Chen P, Wallingford JB, Wynshaw-Boris A (2006a). Dishevelled genes mediate a conserved mammalian PCP pathway to regulate convergent extension during neurulation. Development 133, 1767–1778.
Wang J, Mark S, Zhang X, Qian D, Yoo SJ, Radde-Gallwitz K, Zhang Y, Lin X, Collazo A, Wynshaw-Boris A, *et al.* (2005). Regulation of polarized extension and planar cell polarity in the cochlea by the vertebrate PCP pathway. Nat Genet 37, 980–985.

Wang Y, Guo N, Nathans J (2006b). The role of Frizzled3 and Frizzled6 in neural tube closure and in the planar polarity of inner-ear sensory hair cells. J Neurosci 26, 2147–2156.

Wansleeben C, Feitsma H, Montcouquiol M, Kroon C, Cuppen E, Meijlink F (2010). Planar cell polarity defects and defective Vangl2 trafficking in mutants for the COPII gene Sec24b. Development 137, 1067–1073.

Yap CC, Winckler B (2015). Adapting for endocytosis: roles for endocytic sorting adaptors in directing neural development. Front Cell Neurosci 9, 119.

Yu A, Rual JF, Tamai K, Harada Y, Vidal M, He X, Kirchhausen T (2007). Association of Dishevelled with the clathrin AP-2 adaptor is required for Frizzled endocytosis and planar cell polarity signaling. Dev Cell 12, 129–141.

Zhao X, Jones SM, Yamoah EN, Lundberg YW (2008). Otoconin-90 deletion leads to imbalance but normal hearing: a comparison with other otoconia mutants. Neuroscience 153, 289–299.

Zhao Y, Keen JH (2008). Gyrating clathrin: highly dynamic clathrin structures involved in rapid receptor recycling. Traffic 9, 2253–2264.

Zhen L, Jiang S, Feng L, Bright NA, Peden AA, Seymour AB, Novak EK, Elliott R, Gorin MB, Robinson MS, *et al*. (1999). Abnormal expression and subcellular distribution of subunit proteins of the AP-3 adaptor complex lead to platelet storage pool deficiency in the pearl mouse. Blood 94, 146–155.

Zlatic SA, Tornieri K, L'Hernault SW, Faundez V (2011). Clathrin-dependent mechanisms modulate the subcellular distribution of class C Vps/HOPS tether subunits in polarized and nonpolarized cells. Mol Biol Cell 22, 1699–1715.